Stanford Exploration Project, Report 70, December 18, 1997, pages 1–191

Stanford Exploration Project, Report 70, December 18, 1997, pages 1–191

Elastic parameter estimation by Kirchhoff prestack depth migration/inversion

David E. Lumley and Wafik B. Beydoun[1]

ABSTRACT

Obtaining multiparameter elastic depth images is a key step toward seismic reservoir characterization. We develop a prestack depth migration/inversion (m/i) method which produces such images in two steps. The first step involves a "true amplitude" Kirchhoff elastic prestack depth migration, which provides migrated depth images of the elastic $\grave{P}\acute{P}$ reflectivity R_{pp}, and the associated specular reflection angles θ_{pp}. The second step involves fitting three elastic parameters to the migrated elastic specular reflectivity by use of the Bortfeld linearized approximation to the nonlinear Zoeppritz $\grave{P}\acute{P}$ relation, which results in three migrated elastic parameter depth images of the target zone. We investigate the m/i in terms of stability and choice of parameterization, and calculate quantitative "confidence" images to appraise our results. We find that relative changes in P and S impedances are the most robust parameters for standard surface seismic reflection acquisition geometries, and that little or no unambiguous information regarding density variation is contained in the standard specular illumination range of 0°–30°. Our method is tested with synthetic and field data examples, the latter to be presented at a later date pending proprietary release.

INTRODUCTION

Overview

The structure of this paper will be as follows. First, we give a brief introduction to the present research. In particular, motivations and potential applications of the Kirchhoff migration/inversion method to seismic exploration and reservoir characterization are suggested. Second, we give a very brief outline of the mathematical and physical theoretical concepts to give an intuitive foundation to the overall approach. Next, we demonstrate the technique with a synthetic data application. Several migration and inversion issues are examined using primary synthetic seismograms generated from a reasonable estimate of the true earth model at an actual field survey site. The synthetic results serve as a *control* in terms of what we should and should not expect to recover in the elastic parameter depth images obtained from the field data.

[1]Exploration Research, ARCO Oil and Gas Company, Plano, TX 75075.

Finally, a presentation and interpretation of the field data results will be given at a later date pending proprietary release. Further details are in manuscript preparation for publication and will appear in subsequent SEP reports.

Motivations

Obtaining multiparameter elastic depth images from seismic reflection data is a key step toward seismic reservoir characterization. High-resolution maps of elastic properties may be directly indicative of lithology, physical states such as pressure or temperature, or pore fluid constituents (Parsons, 1986). Careful calibration of seismic attributes to physical properties measured in situ at boreholes can aid in monitoring Enhanced Oil Recovery (EOR) projects, such as steam injection or in situ combustion (Greaves and Fulp, 1987). These examples suggest applications in hydrocarbon exploration (including direct hydrocarbon detection), reservoir extension, and reservoir production.

Furthermore, there is a widespread notion that seismic properties such as P and S impedance may correlate well with other more elusive earth properties, such as porosity, permeability, sand/shale content, or sand thickness. Often, secondary parameters such as porosity are not directly ascertainable from seismic reflection data, but can be measured in situ at reservoir zones. If a few robust parameters can be extracted from seismic reflection data, then perhaps their geostatistical correlations to measured secondary parameters such as porosity can be used to interpolate or extrapolate borehole measurements over a large seismic survey area (Doyen, 1988). These applications suggest implications for reservoir management, including constraints to flow simulations, design and implementation of production and EOR strategies, and refined calculation of net pay volumes. Extracting reliable elastic parameter estimates from seismic reflection data would be an important challenge in achieving these goals.

Elastic parameter depth images

The driving force behind the current research effort is to extract as much information as possible about subsurface physical properties from seismic reflection data. The first and largest part of this effort is to reconstruct the Zoeppritz $\grave{P}\acute{P}$ reflection coefficients, R_{pp}, as a function of specular reflection angle θ_{pp} at each subsurface pixel in the designated target zone. This is accomplished by the Kirchhoff elastic prestack depth migration, which is *elastic* in the sense that background migration model values of V_p, V_s, and ρ are specified. Our method is similar in spirit to that of Parsons (1986), which in turn is based on the methods of Beylkin (1985) and Bleistein (1987), except we consider elastodynamic wave propagation instead of acoustics. Additionally, values of the attenuation quality factor Q may be specified as a function of a single dominant frequency to approximate anelastic exponential amplitude attenuation (but not dispersion). It is a true *depth* migration in the sense that heterogeneous interval model properties, including lateral velocity variations, are specified as a function of *spatial* coordinates, in direct contrast to time migration methods.

Given the Zoeppritz specular reflectivity R_{pp}, information can be further extracted regarding the polarity, magnitude, and spatial distribution of *relative changes* in elastic parameters. Algorithmically, we achieve this inversion by defining a matrix equation relating R_{pp} for several specular angles to three elastic parameters using the linearized Bortfeld approximation to the nonlinear Zoeppritz $\grave{P}\acute{P}$ coefficient (Bortfeld, 1961). The matrix system is then inverted by Singular Value Decomposition (SVD) at each subsurface location. (For a review of the SVD method we refer the reader to Lines and Treitel, 1984.) This allows the possibility of producing elastic parameter depth images of the subsurface target zone, similar in appearance to prestack depth migrations, each exhibiting spatial variations in P or S impedance, for example. Such images will be shown in this report for synthetic data, with the corresponding field data images to be shown at a later date. Ideally, this capability will provide new or additional information about subsurface properties which may be useful in exploration and production applications.

THEORY

This section is intended to give a brief and intuitive overview of the theoretical research we conducted in order to implement the Kirchhoff migration/inversion technique. It is *not* intended to give rigorous derivations or proofs! Readers interested in the latter can refer to Lumley *et al.* (1991), and subsequent SEP reports, in which the full mathematical details are to be expounded.

Elastic specular reflectivity estimation

Let us outline the mathematical and physical components of the true-amplitude elastic migration reflectivity theory. We refer the reader to the paper of Stolt and Weglein (1985) for a comprehensive overview of seismic migration and inversion techniques.

We begin by considering a small *local* neighborhood about a single subsurface location $\mathbf{x_o}$. In general, at $\mathbf{x_o}$ we can define an incident vector displacement wavefield $\mathbf{u}^{\text{I}}$ and a scattered vector displacement wavefield $\mathbf{u}^{\text{S}}$. The wavefield $\mathbf{u}^{\text{I}}$ is due to the seismic source (dynamite, Vibroseis, airgun array, etc.), and $\mathbf{u}^{\text{S}}$ contains the scattered reflections and diffractions caused by the source energy bouncing off of rapid changes in subsurface elastic properties, such as reflectors, diffractors and fault zones. The wavefields are vectors since they contain the full three-component directional information of elastic particle displacement, as opposed to directionless measurements of scalar quantities like acoustic pressure. We can define a 3x3 scattering matrix $\mathbf{R}$ which relates the incident source wavefield to the scattered (reflected or diffracted) wavefield. At reflectors, the elements of the scattering matrix $\mathbf{R}$ contain the elastic Zoeppritz reflection coefficients $\grave{P}\acute{P}$, $\grave{P}\acute{S}$, $\grave{S}\acute{S}$, etc. Hence, if we can determine any of these coefficients, they will in turn reveal information about the changes in elastic parameters which define them. It is evident that determining these coefficients depends on our ability to reconstruct the source wavefield $\mathbf{u}^{\mathrm{I}}$ and the scattered wavefield $\mathbf{u}^{\mathrm{S}}$ *locally* at each subsurface point $\mathbf{x_o}$.

To reconstruct the incident and scattered wavefields, we mathematically solve the elastodynamic wave equation which describes the propagation of elastic waves through heterogeneous media (Aki and Richards, 1980). The mathematical technique used is the Kirchhoff (Love) integral solution (Wu, 1989), which gives a way to reconstruct the wavefields in terms of integrals over the seismic source and the recorded seismic trace data at the surface. To evaluate the integrals, we need to calculate the traveltimes and amplitudes of the waves from the source to each subsurface point, τ_s and A_s, as well as the traveltimes and amplitudes from each receiver to each subsurface point, τ_r and A_r (Keho and Beydoun, 1988). We calculate these traveltimes and amplitudes numerically in heterogeneous media by raytracing techniques (Červený *et al.*, 1977, Beydoun and Keho, 1987).

The final solutions are integrated in a constant offset implementation to preserve the reflection coefficient estimates as a function of fixed specular angles. This is equivalent to presorting the recorded data into constant offset sections, and then migrating each section separately. In practice we do the sorting internal to the migration computer algorithm, so the input data can originate from arbitrary acquisition geometries. Numerically, the integrals become computer summations over all midpoint coordinates $\mathbf{x_m}$ for a fixed offset $\mathbf{x_h}$. The midpoint sum for the R_{pp} coefficient, for a single offset $\mathbf{x_h}$, is

$$R_{pp}(\mathbf{x_o};\mathbf{x_h}) = \sum_{\mathbf{x_m}} \mathbf{W}(A_r, A_s)\cdot\tilde{\mathbf{u}}(\mathbf{x_o},\mathbf{x_m};\mathbf{x_h}, t = \tau_s + \tau_r) \tag{1}$$

or,

$$R_{pp}(\mathbf{x_o};\mathbf{x_h}) = \sum_{\mathbf{x_m}} S_{pp}(\mathbf{x_o},\mathbf{x_m};\mathbf{x_h}, t = \tau_s + \tau_r) \tag{2}$$

where $\mathbf{W}$ is a migration weighting function depending on the raytraced source and receiver amplitudes A_s and A_r, and $\tilde{\mathbf{u}}$ is the recorded trace data which has been deconvolved and filtered. The total factor $S_{pp} = \mathbf{W}\cdot\tilde{\mathbf{u}}$ can be interpreted as a constant offset scattering function, and by summing along the traveltime hyperbolas given by $t = \tau_s + \tau_r$, the summed scatterers make a constant offset reflection.

The specular angles θ_{pp} can be determined by a first moment summation similar to the R_{pp} sum,

$$F(\theta_{pp}(\mathbf{x_o};\mathbf{x_h})) = \frac{\sum_{\mathbf{x_m}} \mid S_{pp} \mid \; F(\theta_i, \theta_s)}{\sum_{\mathbf{x_m}} \mid S_{pp} \mid} \tag{3}$$

where F is some known function like $\cos\theta$, and θ_i and θ_s are the scattering angles made by the incident ray and scattered ray at each subsurface location. The R_{pp} and θ_{pp} results are somewhat similar in spirit to the results of Parsons (1986), which in turn are based on the work of Beylkin (1985) and Bleistein (1987). The main difference is that our method is completely based on the solution to the elastodynamic wave equation in heterogeneous media, as opposed to their acoustic formulations. Several additional theoretical and implementational details further distinguish our work.

So, by implementing the above summations, we obtain estimates of $R_{pp}(\mathbf{x_o}, \mathbf{x_h})$ and $\theta_{pp}(\mathbf{x_o}, \mathbf{x_h})$, which can be combined to obtain $R_{pp}(\theta(\mathbf{x_o}))$; in other words, we can estimate the $\grave{P}\acute{P}$ elastic reflection coefficient as a function of specular reflection angle at every point in the subsurface.

Elastic parameter estimation

Once we have obtained the elastic $\grave{P}\acute{P}$ reflectivity, $R_{pp}(\theta)$, we can consider how to invert for three elastic parameters at each subsurface location.

We begin by making the linear Bortfeld approximation (Bortfeld, 1961, p. 489) to the nonlinear Zoeppritz R_{pp} coefficient (Aki and Richards, 1980, p. 153). This means that we assume that changes in elastic parameters are *linearly* related to reflectivity. In practice, this is a good assumption for elastic parameter changes less than about 20% and specular angles less than about 30° ($\theta = 0°$ is a normal incidence reflection). By elastic parameters, we mean the *change in elastic property divided by the average elastic property* at any given location. In other words, the parameters we estimate are *relative changes* and are *not* absolute magnitudes of properties. Hence we will quote dimensionless values of the parameters, like +10%, instead of +0.2 g/cc (density) or +300 m/s (velocity).

The linearized Bortfeld approximation to $R_{pp}(\theta)$ can be written as

$$R_{pp}(\theta(\mathbf{x_o})) \approx c_1(\theta)P(\mathbf{x_o}) + c_2(\theta)S(\mathbf{x_o}) + c_3(\theta)D(\mathbf{x_o}) \tag{4}$$

where the $c_i(\theta)$ are known coefficients of specular angle (mathematically determined by choice of elastic parameterization), and $\{P, S, D\}$ is the set of three elastic parameters to be found. Generally, P is related to compressional wave properties of the earth, S to shear wave properties, and D to density. At a single location $\mathbf{x_o}$ we have R_{pp} defined for several θ values: as many θ as there are offsets in the recorded data (recall the constant offset summations). The Bortfeld approximation above can then be written as a linear matrix equation

$$\mathbf{A}\mathbf{x} = \mathbf{y} \tag{5}$$

where $\mathbf{A}$ is the matrix of the coefficients $c_i(\theta_j)$, $\mathbf{x}$ is the parameter vector $\mathbf{x} = (P, S, D)^T$, and $\mathbf{y}$ is the corresponding vector of R_{pp} values,

$$\mathbf{y} = (R_{pp}(\theta_1), R_{pp}(\theta_2), \ldots, R_{pp}(\theta_j))^T, \;\; j = 1, N_\theta. \tag{6}$$

If our original data contain 60 offsets (as in a 120 trace per shot standard marine survey), then we will have 60 θ values, $\mathbf{A}$ will be a 60x3 matrix, $\mathbf{x}$ will be the 3x1 parameter vector, and $\mathbf{y}$ will be the 60x1 R_{pp} (data) vector. This is clearly an overdetermined problem since we are using 60 data equations to solve for only 3 parameters. Hence we solve the matrix solution by least squares with a technique known as Singular Value Decomposition (SVD), which decomposes the system into an orthogonal reference frame and reconstructs an optimal solution by eigenvector methods (Lines and Treitel, 1984). We use the spectrum of the 3 eigenvalues to determine the stability of the solution and to estimate the confidence in the inversion result, as discussed later.

Summary

We have discussed the mathematical and physical development of our theoretical Kirchhoff migration/inversion solution from an intuitive perspective (we hope!).

The Kirchhoff reflectivity estimation is an elastic prestack depth migration. It is *elastic* because it uses the elastic properties V_p, V_s, ρ, and anelastic Q factors in the background migration (velocity) model, and backpropagates the recorded wavefield in accordance with the elastodynamic wave equation, as opposed to the standard but more approximate acoustic wave equation. It is a *depth* migration because it uses interval properties (velocities) specified as a function of *spatial* coordinates, as opposed to time migration and rms velocities specified as a function of a temporal coordinate. This implies that the elastic depth migration will tend to be more correct than acoustic time migration if the elastic interval velocity model is known.

The migration is *true amplitude* in the sense that it can recover the correct relative amplitude reflectivity information, without any special preprocessing of the data, provided the data amplitudes are reliable and the elastic migration model is sufficiently accurate. reliable. The migration can estimate the *elastic Zoeppritz reflectivity coefficients* $R_{ij}(\theta)$ *as a function of specular reflection angle*. The subscripts (i, j) indicate that any of the coefficients $\grave{P}\acute{P}$, $\grave{P}\acute{S}$, $\grave{S}\acute{S}$, etc., can be estimated, although at present only the $\grave{P}\acute{P}$ implementation is available. The $R_{pp}(\theta)$ estimates are theoretically correct for *heterogeneous media* (including lateral velocity variations) that are ray valid (i.e., smoothly varying velocities within the model and each layer, if any). The present implementation is for a 2-D geometry, but the theory is valid for *3-D implementation*, which will be considered in the near future. Finally, the technique is well suited to *flexible acquisition geometries*, and should be adaptable to VSP, crosshole, and other non-standard acquisition geometries.

The elastic parameter inversion is *fast* and *robust*. Several (six at present) *parameterization choices* are available, as well as *confidence estimator maps* which give quantitative measures of the relative confidence in the elastic parameter inversion depth images.

A MARINE SYNTHETIC DATA EXAMPLE

We now present the results of a marine synthetic data example. We examine the behavior of our Kirchhoff elastic prestack depth migration/inversion method using synthetic seismograms calculated from a reasonable estimate of the true earth properties at an actual Gulf of Mexico survey site. In particular, we discuss issues such as the accuracy of estimated specular reflectivity and subsequent elastic properties, the robustness of various elastic parameterization choices, and confidence estimates for the final elastic parameter depth images. The synthetic study serves as a *control* experiment, since much effort is made to simulate the actual marine data recording geometry and earth model, so that we can discover what and what not to expect from the field data. At a later date, pending proprietary data release, we will present four field data prestack depth images of: relative changes in P-impedance, relative changes in S-impedance, a direct hydrocarbon indicator, and an accompanying inversion confidence depth image. The field data results will be briefly interpreted and compared to two drilled gas discoveries within the imaged target zone.

The data

The synthetic example is based on a field data set from the Gulf of Mexico. A well was drilled on location which hit gas, and was logged for sonic velocity and density. The reservoir level is at about 2.960 km depth, and the reservoir sand dips 5°-10°. The target zone chosen to perform the Kirchhoff elastic prestack depth migration/inversion is a 2x2 km image area, which is 1.75-3.75 km in depth (1.5-3.0 seconds on the stacked time section).

A synthetic shot gather was calculated based on a 1-D estimate of the true earth model at this site, as shown in Figure **??**. The synthetics were generated by the paraxial raytracing algorithm PRX87 (Beydoun, 1985, Beydoun and Keho, 1987). The shot gather contains $\grave{P}\acute{P}$ primaries only (no multiples) and includes the amplitude effects of 3-D geometrical divergence, elastic reflection/transmission loss, and high frequency anelastic Q attenuation (but not dispersion). We used a 25 Hz peak frequency zerophase Ricker wavelet to simulate the source waveform.

The 1-D elastic model properties are given in Table 0.1, and plotted in Figure **??**. The eight reflections correspond to prominent events in the raw shot gathers. The shale/gas sand contact at the top of the reservoir is at about 2.6 seconds in the synthetic gather. The later events correspond to the reservoir base and a deeper shale boundary. The recording geometry is identical to the marine field survey: the near and far offsets are 318 m and 3293 m respectively, and the group and shot interval are

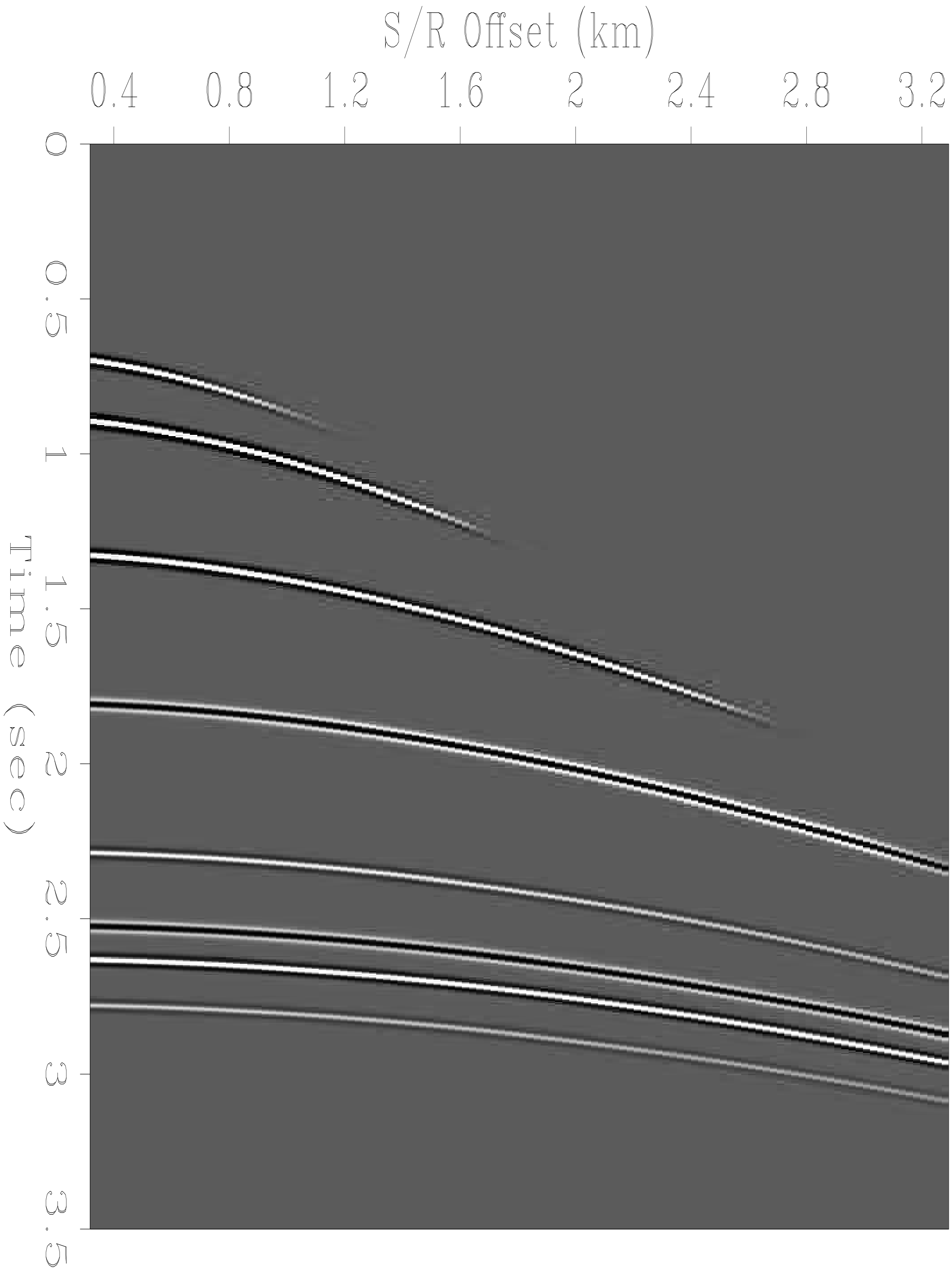

Figure 1: Synthetic shot gather. $\boxed{\text{david2-synth1}}$ [NR]

Depth	**Rock**	**Vp**	**Vs**	ρ	**Q**
630.		1860.	930.	2.04	65
830.		1990.	995.	2.07	75
1330.		2271.	1135.	2.14	97
1960.		2604.	1302.	2.21	128
1970.		2697.	1686.	1.85	137
2610.		2697.	1350.	2.23	137
2960.	shale	2949.	1475.	2.35	164
3110.	gas ss	2770.	1731.	2.00	25
3130.	brine ss	3321.	1660.	2.20	208
3330.	shale	2949.	1475.	2.41	164
4000.		3250.	1625.	2.50	199

Table 0.1: Elastic model for marine synthetics and migration. Physical units are as follows: [Depth] = m, [Vp,Vs] = m/s, [ρ] = g/cc.

both 25 m. The traces are 6.0 seconds in total length (of which we used 3.5 seconds for the m/i), sampled at 4 msec intervals.

The background model

The background anelastic model properties are tabulated in Table 0.1 and plotted in Figure **??**. The model consists of 11 flat layers, each specified by a P-wave and S-wave velocity (V_p, V_s), density (ρ) and P-wave Q value. The V_p values were obtained from a combination of the averaged CMP stacking velocities (after Dix inversion) and the sonic log at the well. The V_s values were calculated above the reservoir using an average V_p/V_s ratio of 2:1, in the absence of hard shear velocity data. The V_s values in the reservoir were extrapolated from values given in an internal ARCO report, based on the same prospect area and similar reservoir conditions (Foster *et al.*, 1990). The density values were calculated using averages from the density well log, and values predicted as a function of the V_p estimates (Gardner *et al.*, 1974). The Q values were predicted as a function of the V_p values (Waters, 1981), except for the reservoir gas sand which was assigned a value of 25 (Batzle, 1991, pers. comm.). The Q values were qualitatively calibrated by estimating two key normal incidence reflection coefficients from the well logs, (the reservoir top at 2960 m depth and a large shallower reflection at 1960 m depth), forward modeling their amplitude response, and comparing to observed amplitudes in the raw shot records. This calibration qualitatively justified the Q values predicted by the Waters relation.

Specular reflectivity estimation

In this section we present the results of inverting the synthetic shot gathers for specular reflectivity. A total of 141 shot gathers is migrated to produce the estimates, which is identical to the field data requirement. The migration model used is identical to the elastic model of Table 0.1 for depths above the gas reflector, but continues through the reservoir zone as a homogeneous halfspace with the properties of the shale layer just above the gas sand. Figure **??** displays the $R_{pp}(z, x_h; \mathbf{x_m})$ elastic $\grave{P}\acute{P}$ estimate, and Figure **??** the $\theta_{pp}(z, x_h; \mathbf{x_m})$ estimate, for a single fixed surface position.

Figures **??** and **??** are *true* common depth point images, as a function of source-receiver offset, as opposed to migrated CMP gathers. Since each gather corresponds to a constant x slice perpendicular to the (x, z) plane (the third dimension being the offset coordinate), reflected events in the true CDP are always flat (provided the velocity model is correct), independent of reflector structure in the (x, z) plane. The near offset traces in Figure **??** have the correct relative $R_{pp}(\theta \approx 0°)$ (peak) amplitudes to within a few percent, as well as the correct Zoeppritz AVO response. The shallow event at 1960 m is a little weak since it is within a Fresnel zone of the mute pattern in the shot gathers. The two reflections beneath the reservoir reflection at 2960 m are somewhat attenuated due to the low Q values in the gas zone which are not present in the migration model. Figure **??** is a contoured version of an identical gather to Figure

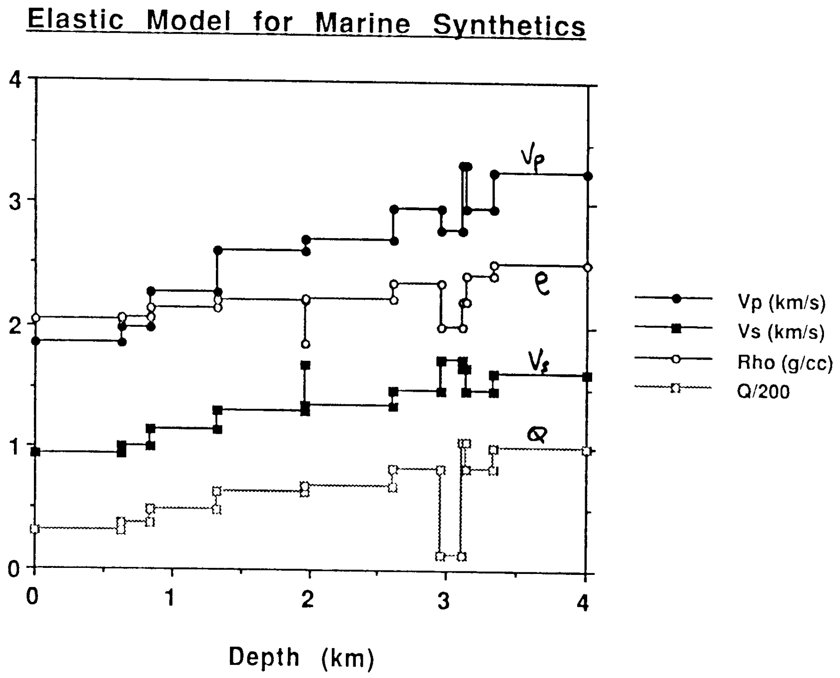

Figure 2: Elastic model for marine synthetics and migration. $\boxed{\text{david2-emodel}}$ [NR]

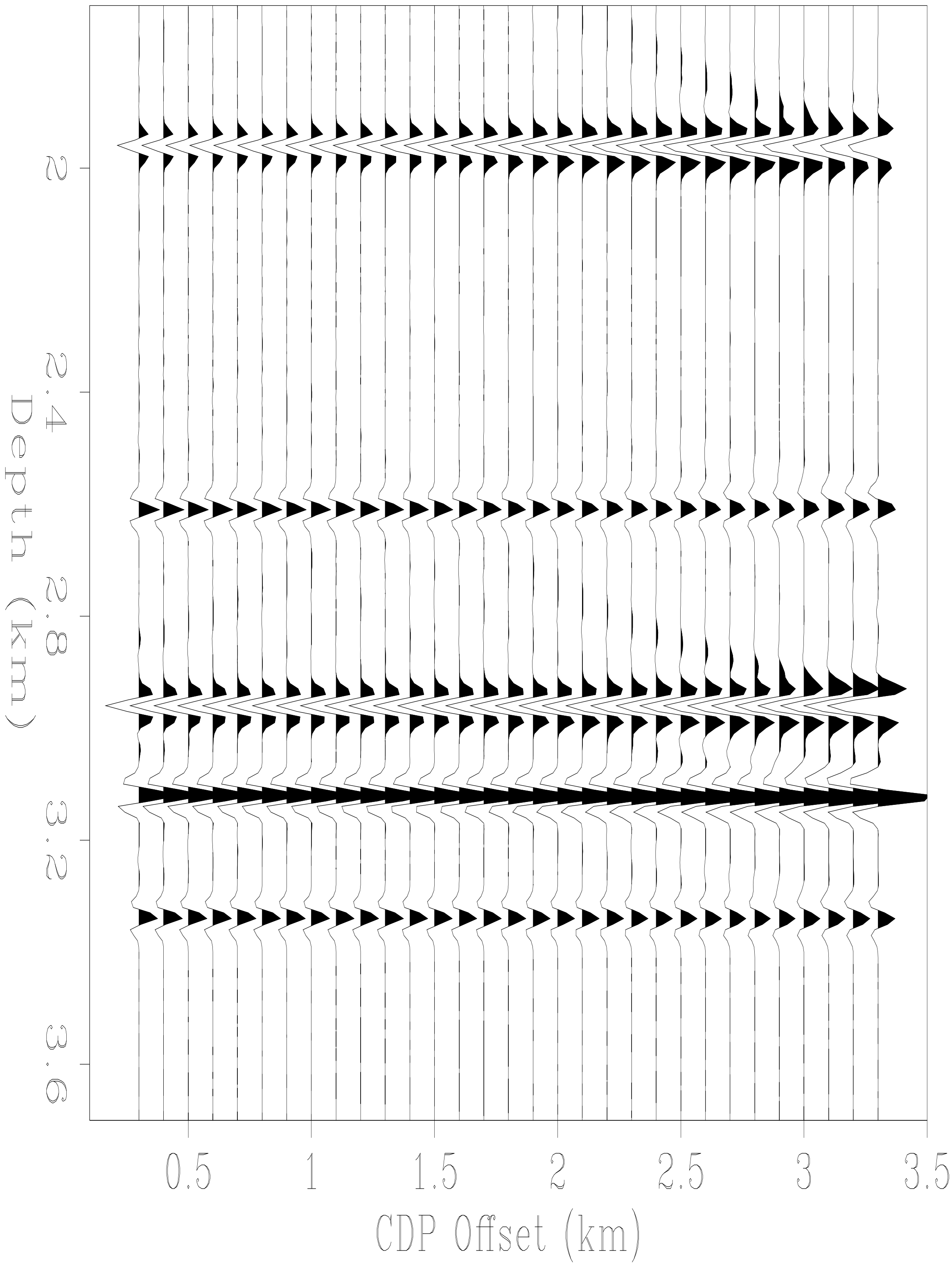

Figure 3: $R_{pp}(x_h, z; \mathbf{x_m})$; migration of marine synthetics. $\boxed{\text{david2-Rpp}}$ [NR]

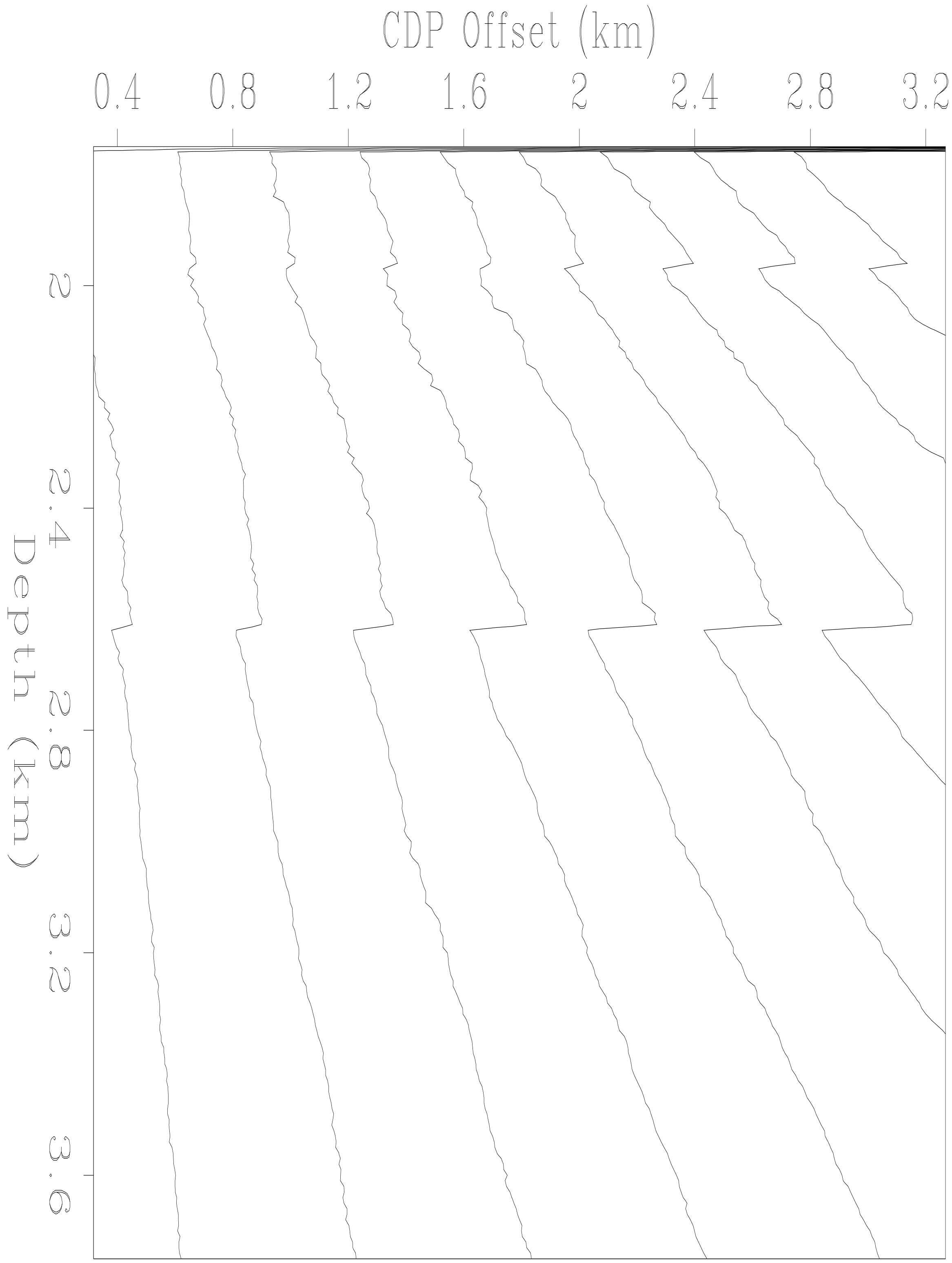

Figure 4: $\theta_{pp}(x_h, z; \mathbf{x_m})$; marine field data migration. The contours represent specular reflection angle in 5° increments, starting with a 5° contour at the nearest offset. david2-theta [NR]

??, except it displays the calculated θ_{pp} specular angles as a function of depth and source-receiver offset. (This is actually the θ_{pp} estimate from the raw field data, since the synthetic θ_{pp} is more difficult to interpret due to large zero-valued areas where no reflections exist). At the reservoir depth, we see that the specular angles of reflection range from about 3° to 33°, which is correct to within 1° compared to raytraced values. The kinks in the contours at 1970 m and 2610 m are accurate evidence of Snell's Law effects on θ_{pp} at abrupt changes in the migration velocity model.

Figure **??** compares the migration estimate of $R_{pp}(\theta)$ at the gas reflection (2960 m) to the true Zoeppritz $\grave{P}\acute{P}$ response as a function of specular angle. The plotted open circles are the correct Zoeppritz values. The filled circles are the migrated $R_{pp}(\theta)$ estimates taken from combining the information in Figures **??** and **??**, after applying a constant scale factor normalization (loss of absolute amplitude in migration: only *relative amplitudes are recoverable*).

The extra curve is a quadratic fit to the estimated $R_{pp}(\theta)$. One can immediately see the good agreement between the correct and estimated Zoeppritz specular reflectivity. This level of accuracy in the migration estimate of R_{pp} on the gas event is representative of the R_{pp} recovery on the other reflection events in the gather. In particular, it is evident that the finite aperture amplitude correction inherent in our method has compensated well for the marine end-on recording geometry in this variable background model. It is important to note that the accurate estimation of R_{pp}, θ_{pp} and the aperture correction are valid for (laterally) heterogeneous media in general.

Finally, some preliminary stability issues in the $R_{pp}(\theta)$ estimation have been investigated. The migration has proved extremely stable in the presence of random noise, certainly up to a s/n level of 2:1. The migration amplitudes are less stable in the presence of reasonable velocity-depth model errors (10%), but acceptable nonetheless. As the velocity-depth errors increase, the kinematic error tends to destroy the amplitude accuracy faster than the error due to geometric divergence (as a function of offset in the R_{pp} gather). This underlines the probable need for good residual migration velocity analysis before inverting $R_{pp}(\theta)$ for elastic parameter variations.

Considering amplitude loss effects, using an acoustic transmission loss model instead of an elastic model produces no error on the normal incidence R_{pp} values (no shear conversions at $\theta \approx 0°$), and less than 10% decrease in amplitude at the far offsets at the target zone. Considering anelastic Q attenuation losses, prescaling the shot gathers with a time-variant rms Q gain function before migration resulted in correct normal incidence amplitudes, but an increase in far offset amplitudes in the target zone of about 100%. Thus, it seems that pre-migration Q amplitude compensation may not be appropriate for preserving migrated $R_{pp}(\theta)$ amplitudes, but rather, the compensation needs to be done properly in the depth model domain during depth migration. Finally, approximations to the WKBJ geometrical divergence amplitude within the migration by simple factors such as $1/r$ or $1/\tau$ produced accurate amplitudes at normal incidence, and were about 10% too weak at far offsets along the

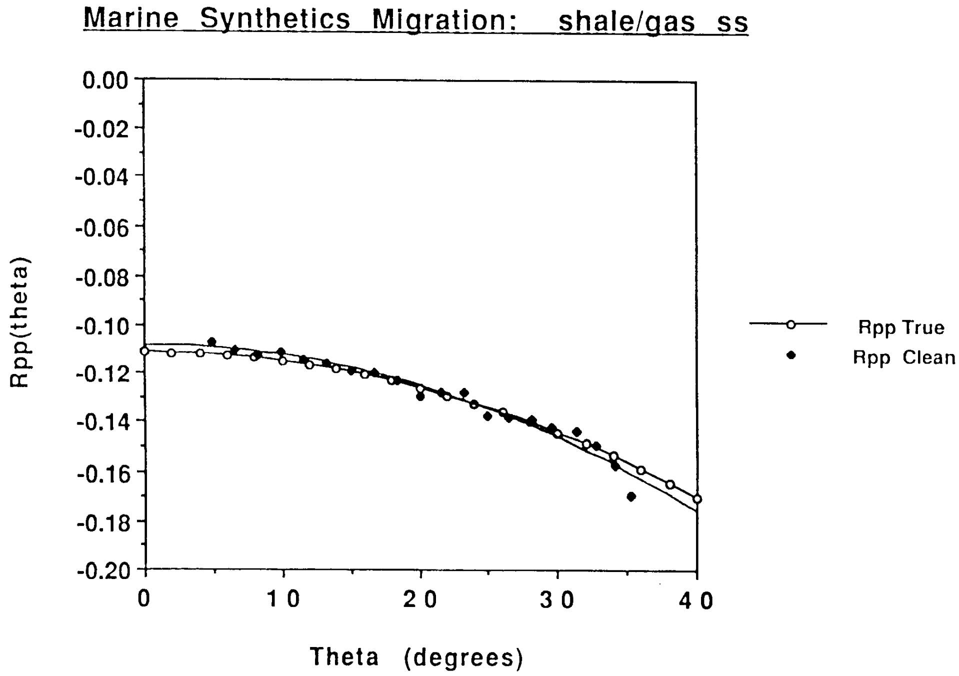

Figure 5: $R_{pp}(\theta)$ *true* vs. $R_{pp}(\theta)$ *estimated* from migrated data. $\boxed{\text{david2-Rtheta}}$ [NR]

gas reflection. Although this error will increase for targets shallower than 3000 m, the approximation seems acceptable for this earth model and acquisition geometry. However, performing a time-variant divergence correction as a function of the *rms* velocity ($V_{rms}^2\tau$) greatly overemphasized the far offset amplitudes. Hence, as with Q compensation, it seems most reasonable to make approximate compensation for geometric divergence in the spatial domain (*depth* migration), and *not* in the time domain (*time* migration).

Elastic parameter estimation

This section describes the inversion of a single R_{pp} and θ_{pp} offset gather by SVD to produce a single depth trace each of P-impedance (I_p), S-impedance (I_s), and density (ρ). Recall that these parameters are of the form $\delta m/\bar{m}$, where δm is the *change* in a given property value, and $\bar{m}$ is the *average* property value, i.e. — *relative changes* in elastic material properties.

Figure **??** shows the three elastic parameter traces $I_p(z;x)$, $I_s(z;x)$ and $\rho(z;x)$ (as a function of depth z, for a fixed surface position x). The first depth trace is the P-impedance trace I_p. The correct model values (in %) from Table **??** are plotted in parentheses, adjacent to the m/i estimated peak values. The I_p estimates are seen to be reasonably accurate. Again the first event at 1960 m is weak due to the mute pattern in the shot records affecting the R_{pp} estimation, and the events below the gas (2960 m) are weak due to attenuation through the low Q gas layer. The I_s estimates are also seen to be quite reasonable, although perhaps less robust than I_p. Also, although the I_s relative change of 0% has been correctly estimated at the gas sand, there are wavelet sidelobe artifacts which would make it difficult to resolve in field data situations. A similar situation applies to the impedance change at 3100 m where two closely spaced reflections overlap into one apparent reflection. This is analogous to a thin bed resolution problem and linearized amplitude tuning effects. Although the I_s estimate is correct at 3100 m (somewhat fortuitously), the overlap of two distinct wavelets erroneously suggests a single impedance change of a large negative polarity which is clearly incorrect. Lastly, the density variation is completely unreliable, except for perhaps the 1960 m event which has the correct polarity and roughly approximate amplitude due to its large specular angle coverage ($\sim 45°$). This will be explained further in the next section under the topic of choice of elastic parameterization for the inversion.

In summary, with accurate synthetic data and a realistic recording geometry and background model, we are able to recover very reasonable I_p estimates, somewhat less robust I_s estimates, and very little (if any) information about density variations.

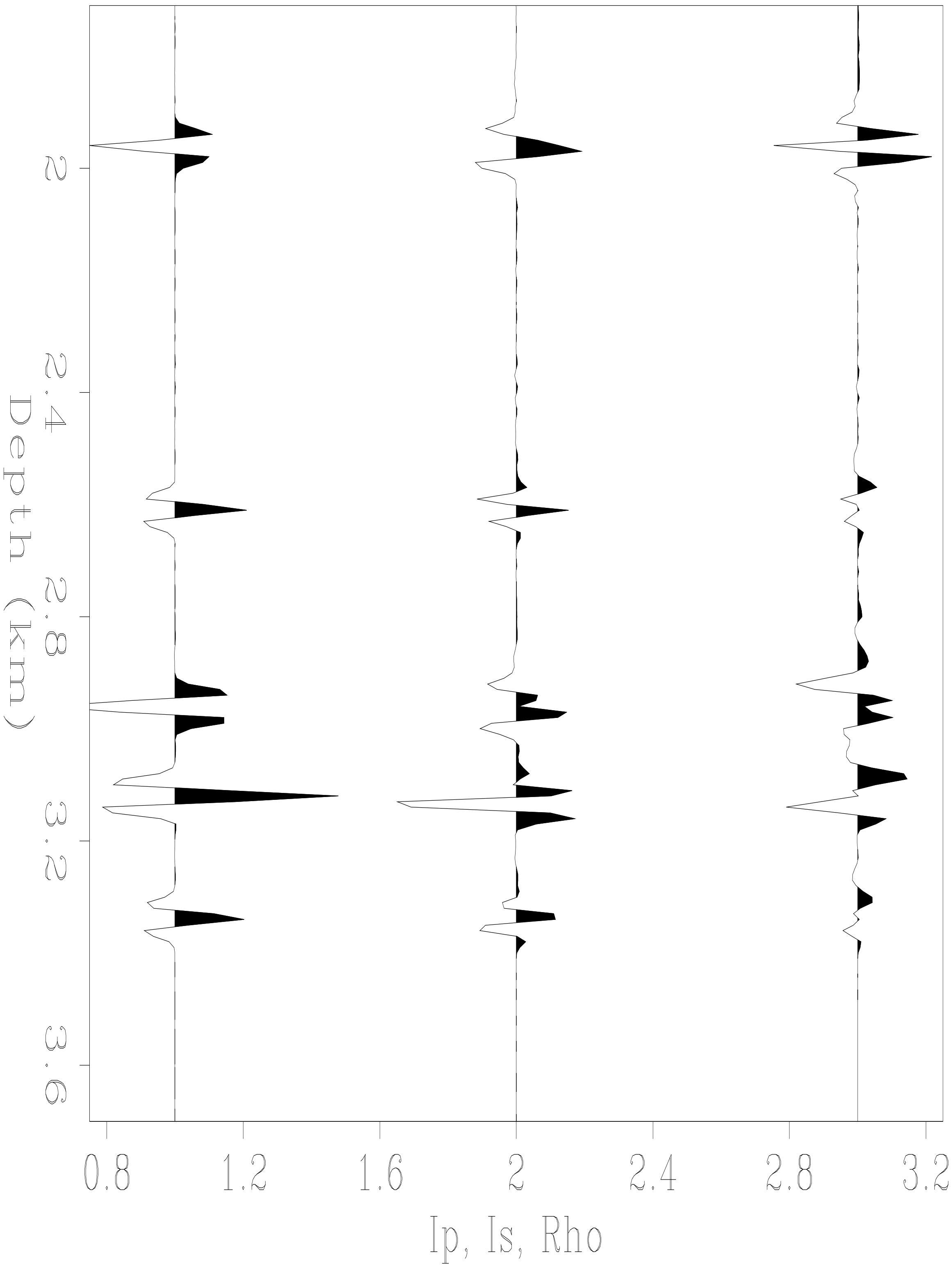

Figure 6: Marine synthetics impedance inversion: I_p, I_s, and ρ. david2-impinv [NR]

Choice of parameterization

In the previous example, we inverted for the elastic impedance parameter set (I_p, I_s, ρ). However, we could have elected to invert for any of several other parameter sets: (V_p, V_s, ρ) for example. We have been investigating six parameter sets so far: Impedance (I_p, I_s, ρ), Velocity (V_p, V_s, ρ), Elastic Modulus (κ, μ, ρ), Lamé Parameter (λ, μ, ρ), V_p/V_s Ratio (I_p, V_p/V_s, ρ), and the so-called "AVO" Parameters (A, B, C). In practice, when we are faced with noisy data given over a limited aperture of specular reflection angles, the issue of parameter choice can become critical, as we will show.

Figures **??** and **??** are plots of "radiation" curves for the Impedance and Velocity parameterizations respectively. A single curve on one plot (I_p in Figure **??** for example) is obtained by making a unit perturbation in that parameter ($\delta I_p/I_p = 1$), and setting the other two parameters in that set to zero ($\delta I_s/I_s = \delta\rho/\rho = 0$). This yields that parameter's coefficient as a function of specular angle $c_i(\theta)$ from the Bortfeld approximation in the Theory section. By plotting all three curves for a parameter set we get Figures **??** or **??**, for example. These curves contain a lot of intuition about how robust a given parameterization will be.

Consider the Impedance radiation curves of Figure **??**. The first thing to notice is that, in terms of amplitude sensitivity to the data ($R_{pp}(\theta)$, I_p is the most sensitive, followed by I_s and lastly ρ. Next, at near offsets R_{pp} is due only to I_p, which tends to make it a robust parameter (no ambiguity or non-uniqueness). As offsets increase to about 30°, any remaining AVO response in R_{pp} not explained by I_p has to be due to I_s, since ρ has zero sensitivity. Hence, the intuition from the radiation curves tells us that there is a clear order in the robustness of the three parameters, ranging from I_p the most robust, to ρ the least robust, that for 0°-30° specular coverage I_p and I_s are well resolved, and that R_{pp} contains no information about density variations for $\theta \leq 30°$.

In contrast, and to make a point, consider the Velocity radiation curves of Figure **??**. At near offsets it is completely ambiguous whether R_{pp} is due to changes in V_p or ρ or both. Worse still, as offsets increase, the V_s and ρ curves are almost parallel. This means that if a change in R_{pp} is not explained by V_p with offset, any inversion scheme will have a difficult time trying to decide if that change is due to V_s, ρ or both, since they both have the same change with offset. In noisy, aperture-limited data, the V_p and ρ parameters will be closely coupled at near offsets, and the V_s and ρ curves will be closely coupled at far offsets (30°), giving rise to what is called parameter *leakage*.

To reinforce this point numerically, we have inverted a noisy version of our previous synthetic example. Figure **??** is the noisy version of Figure **??**, obtained by adding random noise, normally distributed with zero mean and standard deviation equal to one half the near offset peak gas amplitude at 2960 m (s/n = 2/1 defined), filtered to match the wavelet frequency band, and with Markovian type lateral coherency. Table **??** gives the inverted elastic parameter estimates for the Impedance, Velocity, and AVO parameterizations at the shale/gas contact. The error estimates in Table **??**

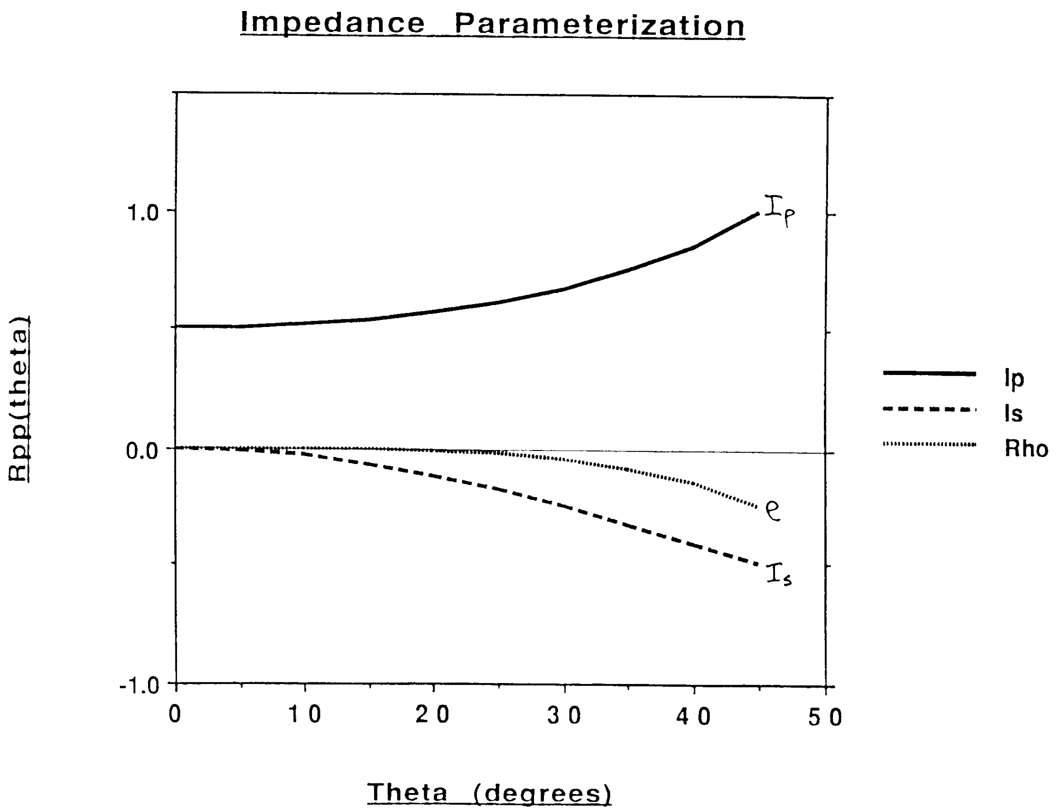

Figure 7: Radiation curves for the Impedance parameterization. david2-imprad [NR]

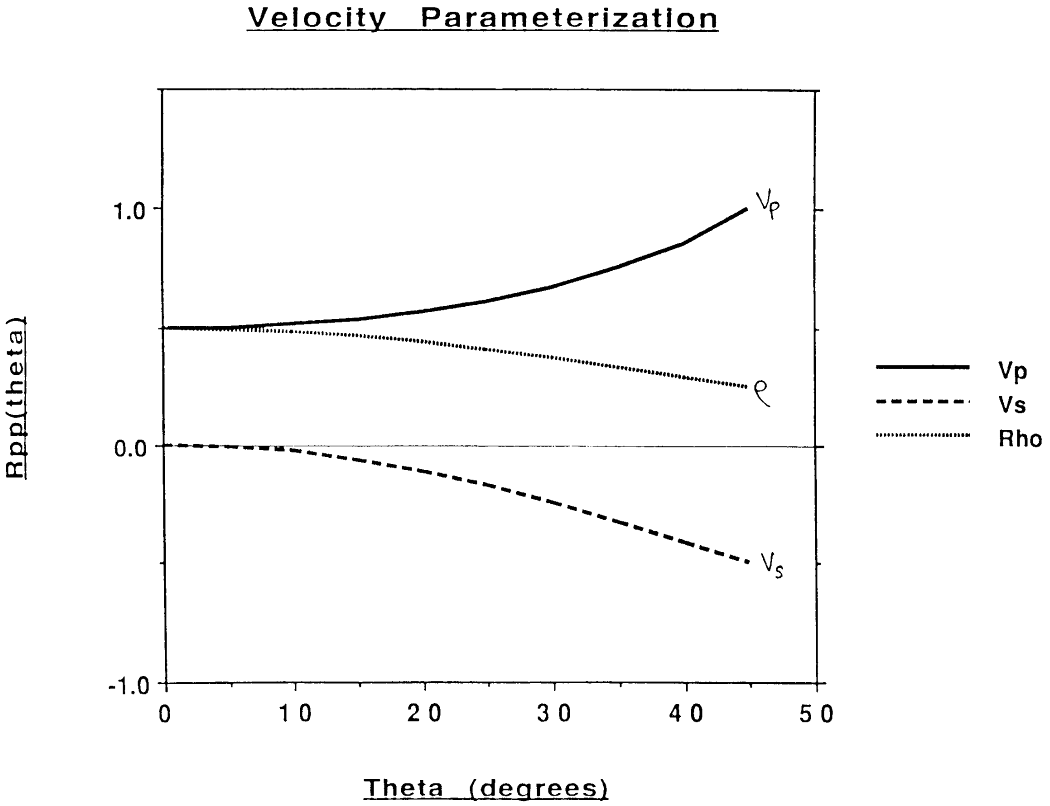

Figure 8: Radiation curves for the Velocity parameterization. $\boxed{\text{david2-velrad}}$ [NR]

are normalized with respect to the standard deviation of the noise in the R_{pp} gather. It is readily evident that our intuitive conclusions from the radiation curves are justified by the impedance and velocity inversion results. For comparison, we have also shown the inversion results with the standard AVO parameterization, which demonstrates a similar order of accuracy in the A and I_p terms, but an inferior accuracy in the B term as compared to I_s. This conclusion is intuitively supported by the AVO radiation curves, which are not shown here.

We are actively developing methods to quantify the optimality of certain parameter sets in terms of inversion stability, parameter sensitivity, and parameter accuracy. This work is in preparation for journal publication. At this point, we recommend the Impedance parameterization for robust elastic parameter inversion, given reflection data acquired with a specular angle range of about 0°-35°.

Inversion "confidence" estimation

The previous section has illuminated the fact that the accuracy of inversion results can vary depending on parameter choice, data noise levels, and incomplete coverage of a target zone constrained by acquisition geometry. In this section we briefly address the issue of estimating a quantitative "confidence" criterion to display alongside elastic parameter inversions. We believe our confidence maps can be of great aid to guiding interpretations of inversion results. This work is a currently ongoing part of our active research, and is in preparation for journal publication.

Figure **??** is the impedance inversion of the noisy gather (Figure **??**), tabulated in Table **??**, and should be compared to the noise-free inversion in Figure **??**. It is immediately obvious from Figure **??** that I_p is the most robust parameter to noise, followed by I_s, followed by ρ. This agrees with our intuitive interpretation of the Impedance radiation curves (Figure **??**), and the values tabulated in Table **??**. It is evident that there are many false impedance changes in the inversion which are caused by noise. We have developed a confidence measure which helps to discriminate real from false impedance changes, and an overall quantitative measure of the inversion's stability at each subsurface point.

Our inversion confidence estimates for the results of Figure **??** are displayed in Figure **??**. Immediately, one can recognize from the confidence maps that only four events on the inversion traces are of reliable merit. These correspond to four of the five correct events in the synthetic model. The fifth event at 1960 m has low confidence because the random noise has severely contaminated its AVO response as shown in Figure **??**. Comparison of the lateral coherency and amplitude of events in Figure **??** qualitatively reinforces the relative quantitative confidence estimates in Figure **??**. However, the peak confidence value is about 30%, which indicates that on the whole, the inversion is having trouble with the noise level and coherency. Furthermore, it is evident that the confidence in I_p is about six times greater than the confidence in I_s, and there is little or no confidence in any of the density variations. Finally, a

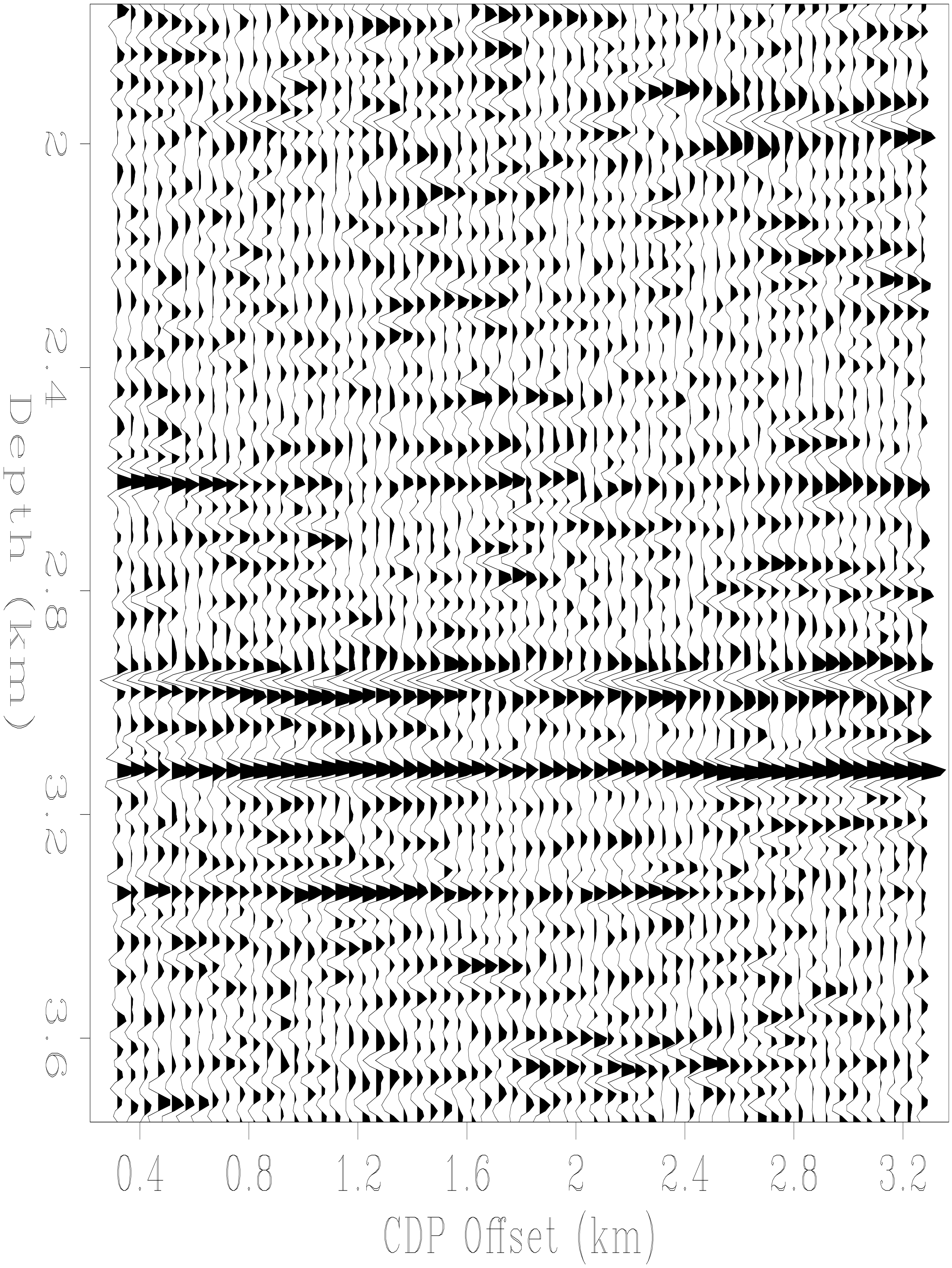

Figure 9: Noisy synthetics with 50% filtered Gaussian spatially coherent noise. $\boxed{\text{david2-Rnoise}}$ [NR]

Elastic Parameter Inversion: s/n=2 Noise Test

(Shale / Gas SS @ 3000 m)

Impedance

Inaccurate:	Ip= -20.8	Is= -06.8	Rho= -03.2
Accurate:	Ip= -22.0	Is= +00.0	Rho= -16.0
Error:	E1= 5%	E2= 31%	E3= 58%

"AVO"

Inaccurate:	A= -11.1	B= -01.4	C= -01.1
Accurate:	A= -11.0	B= -11.0	C= -16.0
Error:	E1= 1%	E2= 87%	E3= 135%

Velocity

Inaccurate:	Vp= -11.2	Vs= +00.8	Rho= -10.8
Accurate:	Vp= -06.0	Vs= +16.0	Rho= -16.0
Error:	E1= 47%	E2= 138%	E3= 47%

Figure 10: Elastic parameter inversion results for noisy synthetics. david2-table2 [NR]

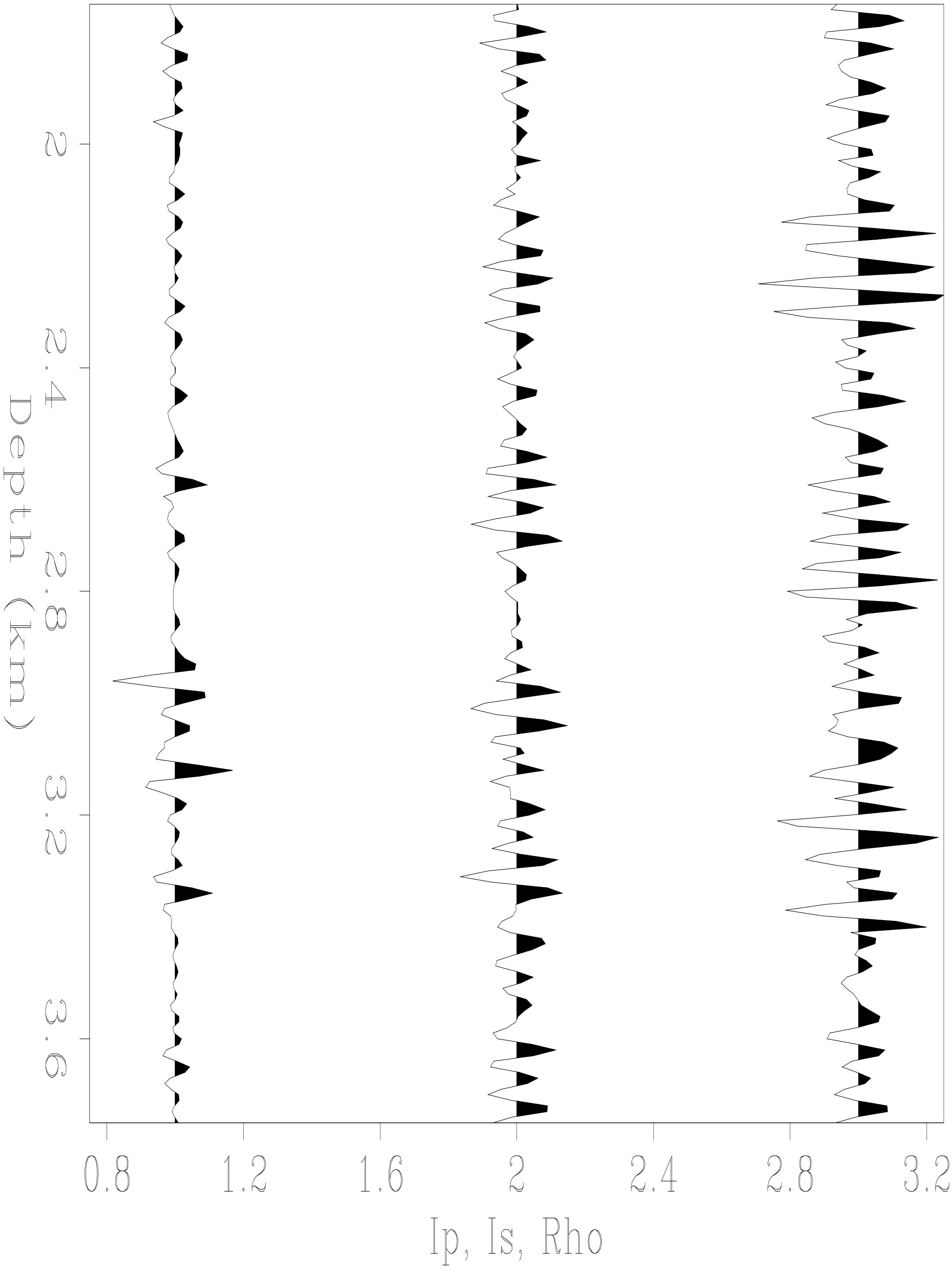

Figure 11: Noisy marine synthetics impedance inversion: I_p, I_s, and ρ. david2-invnoise [NR]

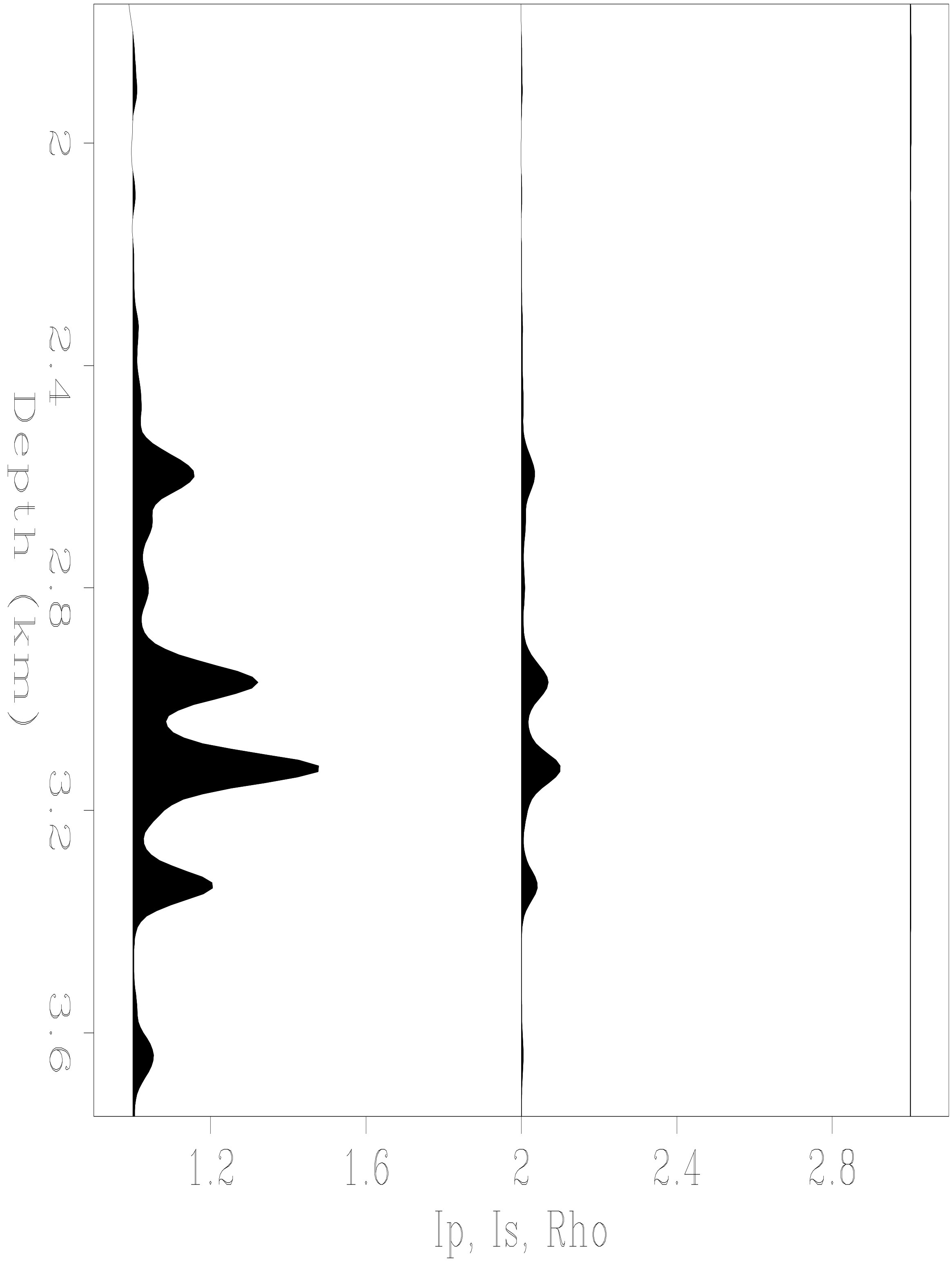

Figure 12: Impedance inversion “confidence” map for noisy synthetics. david2-conf [NR]

false event due to coherent noise at 3650 m is given some nonzero confidence because of its coherency in the R_{pp} gather as shown in Figure **??**. Hence, our confidence estimates can greatly aid in the appraisal of inversion results (evaluating their worth and reliability from one location to another), but are not immune to noise which is coherently correlated with reflection events.

We now briefly describe the confidence criteria from a general perspective. Readers interested in more detail can request a paper preprint from the authors, or stay tuned for subsequent SEP reports. The confidence measure consists of objective numerical criteria calculated directly from the R_{pp} data and the inversion step. From the R_{pp} data, we calculate quantitative measures of event coherency and average coherent amplitude, as a function of offset. During the inversion step, we calculate the "goodness of fit" of the parameter estimates to the R_{pp} values, and the eigenvalue spectrum stability of the matrix system, at each subsurface location. The confidence estimate is a function of these measures. A confidence value of 100% means implies maximum offset coherency and amplitude in the CDP gather, as well as a perfect fit of the parameter estimate to the data, and maximum stability in the singular value decomposition.

CONCLUSIONS

We have developed a Kirchhoff prestack depth migration method which is consistent with elastic wave propagation through a background model in which one can specify values of P-wave velocity (V_p), S-wave velocity (V_s), density (ρ), and the anelastic attenuation factor (Q). The method correctly estimates the $\grave{P}\acute{P}$ Zoeppritz elastic reflectivity coefficient R_{pp}, and the associated specular reflection angles θ_{pp}, in synthetic studies based on an actual field data application with drilling information. This method is a true amplitude *depth* migration in that the R_{pp} and θ_{pp} estimates are valid for laterally heterogeneous velocity models. The algorithmic implementation is computationally efficient in that it takes 6.0 cpu hours on a Sun Sparcstation 1^+ to migrate 140 marine shot gathers (16,800 traces) into a 2x2x3 km^3 target depth image volume (1 million pixels) in a 1-D background model, each of R_{pp} and θ_{pp} as a function of depth, horizontal distance and source-receiver offset. However, this time can increase significantly for complex 2-D migration velocity models which require intense raytracing calculations.

A method has also been developed to invert $R_{pp}(\theta)$ gathers in order to produce depth images of subsurface elastic parameter variations. Parameterization choice issues have been investigated, and it has been found that the Elastic Impedance parameter set (I_p, I_s, ρ) is the most robust set for our purposes. The other less favorable parameterizations investigated were Velocities, Elastic Moduli, Lamé Parameters, V_p/V_s Ratio, and the industry-standard "AVO" Parameterization (A, B, C). In all parameterizations, local *relative changes* in elastic properties are recovered, and not the elastic property values themselves. A quantitative measure of "confidence" has been developed to appraise the quality of the inversion images. Both the elastic parameter inversion and confidence criterion methods have been successfully tested on synthetic data and validated through the field data application. The elastic parameter inversion takes about 10 cpu minutes on a Sun Sparcstation 1^+ for the field data application discussed in this report.

Further details concerning the migration/inversion method, the confidence estimates, and the field data results are in preparation for journal publication, and are likely to appear in subsequent SEP reports (pending proprietary data release).

ACKNOWLEDGMENTS

We thank Tim Keho and Arthur Weglein of ARCO Research for their constructive discussions. The paraxial raytracing algorithm PRX87 was kindly made available by Arthur Cheng and Nafi Toksoz at the Earth Resources Lab, Massachussetts Institute of Technology. Finally, we thank ARCO Oil and Gas Company for supporting this research.

REFERENCES

Aki, K., and Richards, P. G., 1980, Quantitative seismology, **1**: W. H. Freeman and Company, San Francisco.

Batzle, M., 1990, Personal communication: Exploration Research, ARCO Oil and Gas Company, Plano, Texas.

Beydoun, W. B., 1985, Asymptotic wave methods in heterogeneous media: Ph.D. Thesis, Massachussets Institute of Technology.

Beydoun, W. B., and Keho, T. H., 1987, The paraxial ray method: Geophysics, **52**, 1639-1653.

Beylkin, G., 1985, Imaging of discontinuities in the inverse scattering problem by inversion of a causal generalized Radon transform: J. Math. Phys., **26**, 99-108.

Bleistein, N., 1987, On the imaging of reflectors in the earth: Geophysics, **52**, 931-942.

Bortfeld, R., 1961, Approximations to the reflection and transmission coefficients of plane longitudinal and transverse waves: Geophysical Prospecting, **9**, 485-502.

Červený, V., Molotkov, I. A., and Pšenčík, I., 1977, Ray method in seismology: Univerzita Karlova, Praha.

Doyen, P. M., 1988, Porosity from seismic data – a geostatistical approach: Geophysics, **53**, 1263-1275.

Foster, D. J., Hong, M. R., Ley, R., Shellenbaum, B., Smith, S. W., Swan, H., and Wattrus, N., 1990, AVO task force – part 1: ARCO Internal Research Report RR 90-0022, Exploration Research and Technical Services, ARCO Oil and Gas Company.

Gardner, G. H. F., Gardner, L. W., and Gregory, A. R., 1974, Formation velocity and density – the diagnostic basics for stratigraphic traps: Geophysics, **39**, 770-780.

Greaves, R. J., and Fulp, T. J., 1987, Three-dimensional seismic monitoring of an enhanced oil recovery process: Geophysics, **52**, 1175-1187.

Keho, T. H., and Beydoun, W. B., 1988, Paraxial ray Kirchhoff migration: Geophysics, **53**, 1540-1546.

Lines, L. R., and Treitel, S., 1984, Tutorial – a review of least-squares inversion and its application to geophysical problems: Geophysical Prospecting, **32**, 159-186.

Lumley, D. E., Beydoun, W. B., and Oldenburg, D. W., 1991, Elastic specular reflectivity estimation by Love–WKBJ integration of seismic waveforms: Geophysical Journal International, in preparation.

Parsons, R., 1986, Estimating reservoir mechanical properties using constant offset images of reflection coefficients and incident angles: Expanded Abstracts of the SEG.

Stolt, R. H., and Weglein, A. B., 1985, Migration and inversion of seismic data: Geophysics, **50**, 2458-2472.

Waters, K. H., 1981, Reflection seismology – a tool for energy resource exploration: Wiley-Interscience, New York.

Wu, R., 1989, Representation integrals for elastic wave propagation containing either the displacement term or the stress term alone: Physical Review Letters, **62**, 497-500.